ACTA MECHANICA SINICA (English Series), Vol.19, No.1, February 2003 ISSN 0567-7718
The Chinese Society of Theoretical and Applied Mechanics
Chinese Journal of Mechanics Press, Beijing, China
Allerton Press, INC., New York, U.S.A.

STICTION AND ANTI-STICTION IN MEMS AND NEMS*

ZHAO Yapu (赵亚溥)†

(*LNM, Institute of Mechanics, Chinese Academy of Sciences, Beijing* 100080, *China*)

ABSTRACT: Stiction in microelectromechanical systems (MEMS) has been a major failure mode ever since the advent of surface micromachining in the 80s of the last century due to large surface-area-to-volume ratio. Even now when solutions to this problem are emerging, such as self-assembled monolayer (SAM) and other measures, stiction remains one of the most catastrophic failure modes in MEMS. A review is presented in this paper on stiction and anti-stiction in MEMS and nanoelectromechanical systems (NEMS). First, some new experimental observations of stiction in radio frequency (RF) MEMS switch and micromachined accelerometers are presented. Second, some criteria for stiction of microstructures in MEMS and NEMS due to surface forces (such as capillary, electrostatic, van der Waals, Casimir forces, etc.) are reviewed. The influence of surface roughness and environmental conditions (relative humidity and temperature) on stiction are also discussed. As hydrophobic films, the self-assembled monolayers (SAMs) turn out able to prevent release-related stiction effectively. The anti-stiction of SAMs in MEMS is reviewed in the last part.

KEY WORDS: MEMS, stiction, anti-stiction, work of adhesion, self-assembled monolayer (SAM)

1 INTRODUCTION

As a kind of fundamental catastrophic failure in microelectromechanical systems (MEMS), stiction deserves a careful study. Stiction is a term for the unintentional adhesion of compliant microstructure surfaces when restoring forces are unable to overcome interfacial forces such as capillary, electrostatic, van der Waals, Casimir forces, and other kinds of "chemical" forces[1~6]. The stiction problem of MEMS can be divided into two categories[7]: release-related stiction and in-use stiction. Release-related stiction occurs during the process of the sacrificial layer removal in fabrication of microstructures, and such stiction is caused primarily by capillary forces. In-use stiction usually occurs when successfully released microstructures are exposed to a humid environment.

Figure 1 shows the release-related stiction of a radio frequency (RF) MEMS switch to the substrate[8] due to large surface-area-to-volume ratio. Figure 2 shows the stiction of comb fingers in a micromachined accelerometer by bulk micromachining. Microstructure surfaces may come into contact unintentionally through acceleration or electrostatic forces, or intentionally in applications where surfaces impact or shear against each other. When adhesive attractions exceed restoring forces, surfaces permanently adhere to each other causing device failure: a phenomenon known as in-use stiction. Figure 3 shows the stiction of structural members in an accelerometer after impact loading.

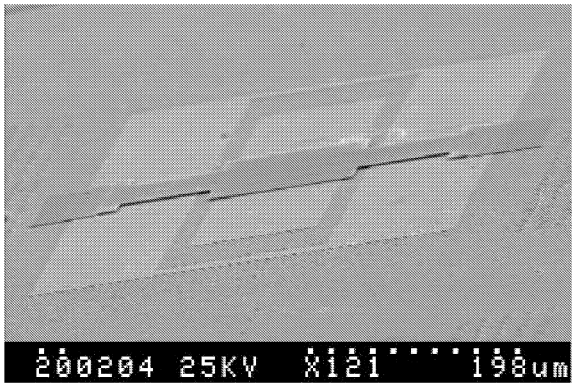

Fig.1 SEM of adhered RF-MEMS switch to substrate obtained by the author's group

Received 9 December 2002
* The project supported by the Distinguished Young Scholar Fund of NSFC (10225209), key project from the Chinese Academy of Sciences (KJCX2-SW-L2) and National "973" Project (G1999033103)
† E-mail: yzhao@lnm.imech.ac.cn

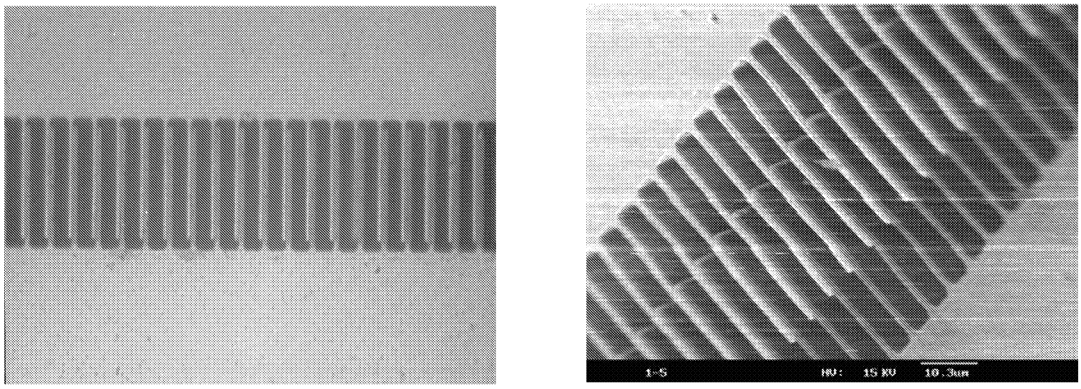

Fig.2 Stiction of the comb fingers in micromachined accelerometers obtained by the author's group

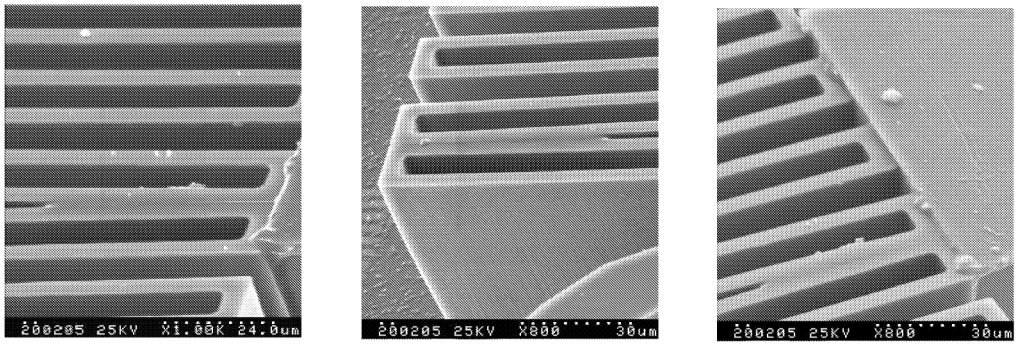

Fig.3 Stiction of microstructural members in an accelerometer after impact loading obtained by the author's group

In the 1990s, considerable effort has been spent on models describing and predicting the stiction properties of surfaces in MEMS in contact. Criteria for stiction of microstructures in MEMS will be briefly reviewed in the first part of this paper. As hydrophobic films, the self-assembled monolayers (SAMs) have been used to prevent release-related stiction effectively, the anti-stiction of SAMs in MEMS are reviewed in the second part of this paper.

2 CRITERIA FOR STICTION OF MICROSTRUCTURES IN MEMS AND NEMS

2.1 Mechanical Collapse Induced by Capillary Force and Elastocapillary Number

Suspended elements in MEMS are typically fabricated by first forming a layer of the plate or beam material on top of a sacrificial layer of another material and then etching away the sacrificial layer. If the etch is performed in a liquid environment, a liquid bridge will be formed between the suspended member and the substrate when the liquid is removed during a dehydration cycle, yielding an attractive capillary force which may be sufficiently strong to make it collapse.

A dimensionless number, called elastocapillary number N_{EC}, has been proposed by Mastrangelo and Hsu[9] to characterize the detachment of the microstructure with the substrate. The microstructure is free of stiction when $N_{\mathrm{EC}} > 1$ and will stick to the substrate when $N_{\mathrm{EC}} < 1$. The elastocapillary number, N_{EC}, can be physically explained as the ratio of elastic restoring energy to the capillary energy. The results of elastocapillary number for different microstructures are summarized in Table 1, with E being the Young's modulus, t the member thickness, h the gap, θ_{c} the contact angle, γ_{l} the liquid surface tension, ν the Poisson's ratio, σ_{R} the residual tensile stress, and l, w, r_0 being the length, width and radius.

Table 1 Approximate elastocapillary numbers for different microstructures

Microstructure	Approximate elastocapillary numbers
cantilever beam	$\dfrac{2Eh^2t^3}{9\gamma_{\rm l}\cos\theta_{\rm c}l^4\,(1+t/w)}$
doubly supported beam	$\dfrac{128Eh^2t^3}{15\gamma_{\rm l}\cos\theta_{\rm c}l^4\,(1+t/w)}\left[1+\dfrac{2\sigma_{\rm R}l^2}{7Et^2}+\dfrac{108h^2}{245t^2}\right]$
circular plate	$\dfrac{10}{9}\left(\dfrac{5}{2}\right)^{2/3}\dfrac{Eh^2t^3}{\gamma_{\rm l}\cos\theta_{\rm c}r_0^4\,(1-\nu^2)}\left[1+\dfrac{3\left(1-\nu^2\right)}{4}\dfrac{\sigma_{\rm R}r_0^2}{Et^2}+\dfrac{2\,187}{2\,560}\left(\dfrac{2}{5}\right)^{2/3}\dfrac{h^2}{t^2}\right]$
square plate	$\dfrac{25Eh^2t^3}{\gamma_{\rm l}\cos\theta_{\rm c}w^4\,(1-\nu^2)}\left[1+\dfrac{2\left(1-\nu^2\right)}{9}\dfrac{\sigma_{\rm R}w^2}{Et^2}+\dfrac{5}{12}\dfrac{h^2}{t^2}\right]$

2.2 Contact Stiction and Peel Number

To study the stiction of movable MEMS microstructures to the substrate, a dimensionless number, termed peel number, was proposed by Mastrangelo and Hsu[9]. The peel number, $N_{\rm P}$, is the ratio of elastic strain energy stored in the deformed microstructure to the work of adhesion between the microstructure and the substrate. If $N_{\rm P}>1$, the restored elastic strain energy is greater than the work of adhesion, and the microstructure will not stick to the substrate. If, on the other hand, $N_{\rm P}\le 1$, the deformed microstructure does not have enough energy to overcome the adhesion between the beam and the substrate.

For a long slender cantilever of thickness t, length l and elastic modulus E suspended at a distance h from the substrate, illustrated in Fig.4(a), the peel number is[10]

$$N_{\rm P}=\frac{3Et^3h^2}{2S^4W_{\rm a}} \tag{1}$$

where S is the crack length, and $W_{\rm a}=\gamma_1+\gamma_2-\gamma_{12}$ is the Dupré adhesion or work of adhesion between the cantilever and the substrate, with γ_1 and γ_2 being the surface energies of the two bodies and γ_{12} the interface energy. For a short cantilever beam with just its tip stuck to the substrate, shown in Fig.4(b), the corresponding peel number is[9,10]

$$N_{\rm P}=\frac{3Et^3h^2}{8l^4W_{\rm a}} \tag{2}$$

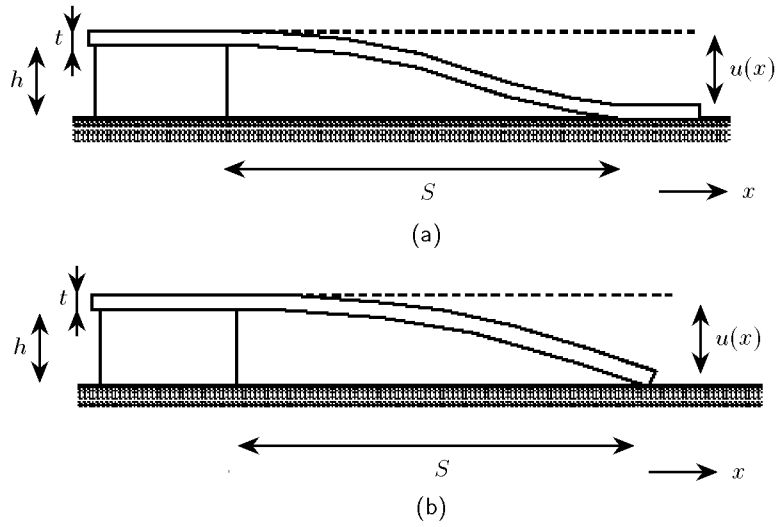

Fig.4 (a) S-shaped cantilever stuck to the substrate over a distance d; (b) Arc-shaped cantilever stuck to the substrate only very near its tip

For a doubly clamped beam, and suspended square and circular plates, the residual stress, σ_{R}, must be considered, and their peel numbers are[9]

$$N_{\mathrm{P}} = \frac{128Et^3h^2}{5l^4W_{\mathrm{a}}}\left[1+\frac{4\sigma_{\mathrm{R}}l^2}{21Et^2}+\frac{256}{2\,205}\left(\frac{h}{t}\right)^2\right]$$

(doubly clamped beam) (3)

$$N_{\mathrm{P}} = \frac{186Et^3h^2}{(1-\nu^2)w^4W_{\mathrm{a}}}\left[1+\frac{27(1-\nu^2)\sigma_{\mathrm{R}}w^2}{310Et^2}+\frac{12}{31}\left(\frac{h}{t}\right)^2\right]$$

(suspended square plate) (4)

$$N_{\mathrm{P}} = \frac{40Et^3h^2}{3(1-\nu^2)r_0^4W_{\mathrm{a}}}\left[1+\frac{51(1-\nu^2)\sigma_{\mathrm{R}}r_0^2}{160Et^2}\right]$$

(suspended circular plate) (5)

where ν is Poisson's ratio, l, w and r_0 are the length of the doubly clamped beam, width of the square plate and radius of the circular plate, respectively.

The maximum dimensions of the microstructures (length of cantilever or doubly clamped beam, width of square plate, and radius of circular plate) that will not stick to the substrate can be obtained from Eqs.(2)~(5) using the threshold condition $N_{\mathrm{P}} = 1$, i.e., the stored elastic strain energy is equal to the work of adhesion. From Eq.(2), the maximum cantilever length that will not stick to the substrate, also called the detachment length, can be determined as

$$l_{\max} = \left(\frac{3Et^3h^2}{8W_{\mathrm{a}}}\right)^{1/4} \tag{6}$$

From Eqs.(3)~(5), the maximum length, width and radius of the fixed-fixed beam, square plate and circular plate are expressed in the same form as follows

$$l_{\max}, w_{\max}, (r_0)_{\max} = \left(\frac{b+\sqrt{b^2+4c}}{2}\right)^{1/2} \tag{7}$$

The corresponding values of b and c in Eq.(7) for different microstructures are presented in Table 2.

Table 2 Coefficients in Eq.(7) for different microstructures

Microstructure	b	c
doubly clamped beam	$\frac{512}{105}\frac{\sigma_{\mathrm{R}}h^2t}{W_{\mathrm{a}}}$	$\frac{128}{5}\left[1+\frac{256}{2\,205}\left(\frac{h}{t}\right)^2\right]\frac{Et^3h^2}{W_{\mathrm{a}}}$
square plate	$\frac{5\,022}{301}\frac{\sigma_{\mathrm{R}}h^2t}{W_{\mathrm{a}}}$	$\left[1+\frac{12}{31}\left(\frac{h}{t}\right)^2\right]\frac{186Et^3h^2}{(1-\nu^2)W_{\mathrm{a}}}$
circular plate	$\frac{17}{4}\frac{\sigma_{\mathrm{R}}h^2t}{W_{\mathrm{a}}}$	$\frac{40Et^3h^2}{3(1-\nu^2)W_{\mathrm{a}}}$

Measurements by Mastrangelo and Hsu[9] were made on an array of beams with different lengths, to find out the longest beam that was not stuck to the substrate (see Fig.5). These cantilevers, close to the transition from sticking to not sticking and vice versa, are arc-shaped. The measurement depends largely on the local properties of the surface near the tip.

Consider the elastic contact of the cantilever and substrate with interface roughness. The surface roughness is represented by asperities, which are modeled as spherical caps with the same radius of curvature R, and the heights of these asperities obey the Gaussian distribution

$$\varphi(z) = \frac{1}{\sqrt{2\pi}\sigma}\exp\left(-\frac{z^2}{2\sigma^2}\right) \tag{8}$$

where σ is the standard deviation of the distribution of asperity heights. The corresponding peel number for cantilever beam adhesion to a rough surface is[11]

$$\bar{N}_{\mathrm{P}} = \frac{N_{\mathrm{P}}}{f(\theta)} \tag{9}$$

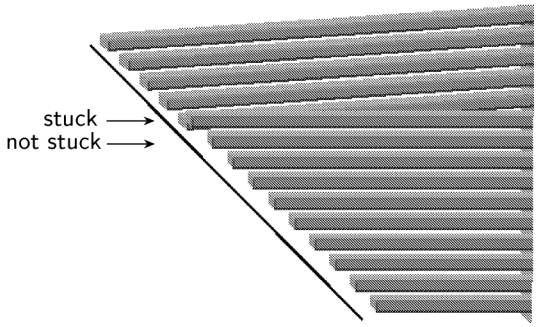

Fig.5 Cantilever beam array (CBA) technique to determine the detachment length

where N_{P} is the peel number for smooth contact (Eq.(1) or Eq.(2)), $\bar{N}_{\mathrm{P}}$ is the peel number considering the rough contact, and

$$f(\theta)=C\int_{s_e}^{\infty}\left[\frac{4\theta}{3\sqrt{2\pi}}\int_{s}^{\infty}(x-s)^{3/2}\exp\left(-\frac{x^2}{2}\right)\mathrm{d}x-\sqrt{2\pi}\int_{s}^{\infty}\exp\left(-\frac{x^2}{2}\right)\mathrm{d}x\right]\mathrm{d}s \tag{10}$$

is a dimensionless roughness function reflecting the influence of surface roughness on stiction (Fig.6), and

$$\theta=\frac{E^*}{W_{\mathrm{a}}}\sqrt{\frac{\sigma^3}{R}} \tag{11}$$

is the adhesion parameter[12] and E^* is the equivalent Young's modulus given by $1/E^*=\left(1-\nu_1^2\right)/E_1+\left(1-\nu_2^2\right)/E_2$.

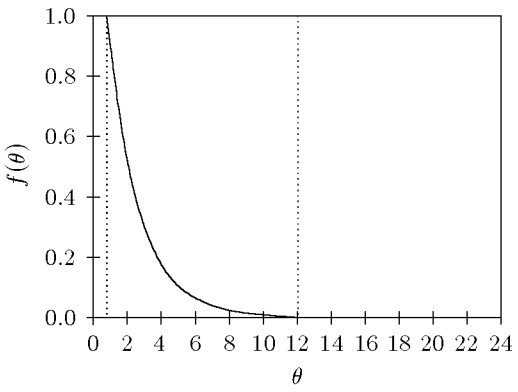

Fig.6 Influence of adhesion parameter on the dimensionless roughness function $f(\theta)$, which decreases monotonically with the adhesion parameter θ

Equation (9) indicates[11] that the stiction of a cantilever beam with a rough substrate is reduced with increasing adhesion parameter θ. The peel number for doubly clamped beam, and suspended square and circular plates with surface roughness can be obtained in the same manner. The design parameters in Eqs.(6) and (7) should be modified accordingly, for example, the maximum cantilever beam length that will not stick to the substrate, or detachment length considering surface roughness, can be modified to

$$l'_{\max}=\left(\frac{3Et^3h^2}{8W_{\mathrm{a}}f\left(\theta\right)}\right)^{1/4} \tag{12}$$

The difference between $l'_{\max}$ and $l_{\max}$ in Eq.(6) is $f\left(\theta\right)$. Noticing the fact that the dimensionless roughness function is less than 1 by referring to Fig.6, then $l'_{\max}$ is always larger than $l_{\max}$. Thus, surface roughness indeed increases the detachment length.

2.3 Stiction by van der Waals and Casimir Forces

Buks and Roukes[13] measured the adhesion between gold surfaces using a micromachined cantilever beam. The adhesion is caused by the Casimir force with a gap of a few micrometers between the cantilever and the substrate. The Casimir force for a small separation is reduced to the nonretarded van der Waals forces[14] with interaction energy per unit area as

$$U=-\frac{A}{12\pi a^2} \tag{13}$$

where A is the Hamaker constant. For the case of Au, it was found[13] that Eq.(13) was a good approximation for a gap $a<2\,\mathrm{nm}$ and the Hamaker constant was measured to be $A=4.4\times10^{-19}\,\mathrm{J}$.

Casimir force has been associated with van der Waals forces. The following comparisons between Casimir and van der Waals forces have been made by Lifshitz:

(1) van der Waals force: Approximation of perturbation theory applied to electrostatic interaction of two dipoles. Valid only when the separation $a<\lambda$, with λ being the retardation length, and corresponding to the transition between the ground and the excited states of the atom. The attraction is proportional to $1/a^3$ and is affected by material properties.

(2) Casimir force: When the separation $a\sim\lambda$ or $a>\lambda$, retardation effects enter. The attraction is proportional to $1/a^4$ and is not affected by material properties.

Thus the Casimir forces take effect at longer distances than the van der Waals forces. Figure 7 shows the calculated results of Casimir and van der Waals energies for two thick films[15]

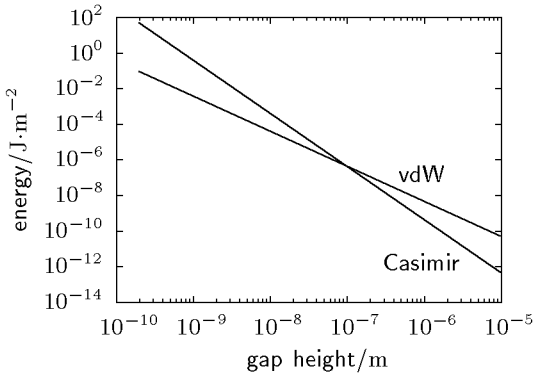

Fig.7 Comparison of van der Waals and Casimir forces for thick gold films[16]

$$E_{\mathrm{vdW}}(a) = 0.28\frac{\hbar\omega_{\mathrm{p}}}{16\pi\sqrt{2}a^2}$$
$$E_{\mathrm{Casimir}}(a) = \frac{\pi^2\hbar c}{720a^3} \tag{14}$$

where $\hbar$ is the Planck's constant divided by 2π, and is equal to 1.055×10^{-34} J·s, ω_{p} is the plasma frequency, a is the gap height, and c is the speed of light and is equal to $2.988\times10^{8}\,\mathrm{m\cdot s^{-1}}$. The crossing point in Fig.7 is at about 100 nm gap height for $\omega_{\mathrm{p}} = 10^{16}$ Hz. As the surfaces get closer together, van der Waals forces and electron exchange interactions dominate.

The Casimir force acting on two parallel uncharged plates with a separation a, in vacuum is given by[6,16]

$$F(a) = -\frac{\pi^2}{240}\frac{\hbar c}{a^4}S \tag{15}$$

where $S \gg a^2$ is the area of plates. Thus movable components in NEMS devices fabricated at distances less than 100 nm between each other often stick together due to strong Casimir force. Serry et al.[17] studied the criterion for adhesion of a $2\,\mu$m thick highly doped single crystal Si microfabricated rectangular membrane strip with a parallel fixed surface in terms of Casimir force as shown in Fig.8. Due to proximity to the rigid flat surface S of the bottom plate, the strip is subject to the attractive Casimir force, and deflects into a curved shape. Numerical simulation showed that for those systems which exhibited adhesion-free stable equilibrium state, the deflection at middle of the strip was always less than $0.48w_0$, with w_0 being the initial gap between the rectangular strip and the parallel surface. However, Serry et al. do not discuss the building of the structure studied or how the deflection of the strip was measured[17].

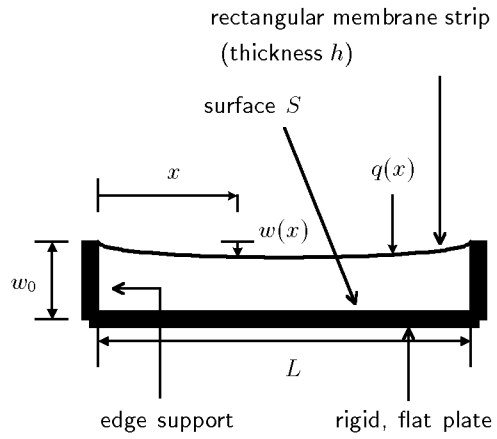

Fig.8 Illustration of the Casimir effect between a rectangular membrane strip and the substrate. $w(x)$ is the deflection of the strip, $q(x)$ is the load, and w_0 is the initial separation between the strip and the substrate

A theoretical analysis[18] has been presented recently of three forces on cantilevers in MEMS, namely acceleration, Casimir and Coulomb forces. This analysis provided theoretical limits to cantilever lengths free from adhesion with substrate. The influence of environmental conditions (relative humidity and temperature) and surface roughness on stiction has been studied theoretically in Ref.[19], which shows that temperature may have a profound effect on stiction at low relative humidity levels, but are less important at high humidity levels.

3 ANTI-STICTION IN MEMS AND NEMS

In order to reduce the release-related stiction, a few engineering methods have been suggested and have proven to be successful. These methods[2] include texturing the surfaces to reduce the contact area (an example[20] is shown in Fig.9, where a periodic array of small supporting post, commonly known as "dimples" has been introduced. This method was first used by Fan[21] for the construction of a micromotor.) and changing surface hydrophobicity, and the avoidance of liquid-vapor interfaces altogether through supercritical fluid, freezing sublimation drying or dry-release methods. Effective measures to prevent in-use sticiton include surface roughening and surface coating with low surface-energy materials, or chemical passivation (e.g., self-assembly monolayers (SAMs) coatings[7,22], diamond-like carbon (DLC) coatings[22,23]). The hydrophobic surface of SAM-coatings prevents the water layer and thereby the capillary forces from forming between two surfaces[24].

A more effective chemical modification for anti-stiction treatments involves the application of a molecular film to the micromachine surface. The term, self-assembled monolayer (SAM), denotes the single layer of ordered molecules adsorbed on a substrate due to bonding between the surface and molecular head group[25]. The SAM consists of a head group and alkyl chain. The head group of the SAM chemisorbs on the special substrate. Thiol chemisorbs on a metal surface such as gold, and silane chemisorbs with the hydroxyl group on silicon or silicon nitride. Indeed, it has been demonstrated that self-assembled monolayer (SAM) coatings deposited from solution may have the following characteristics when properly integrated into the microstructure release process[1]:

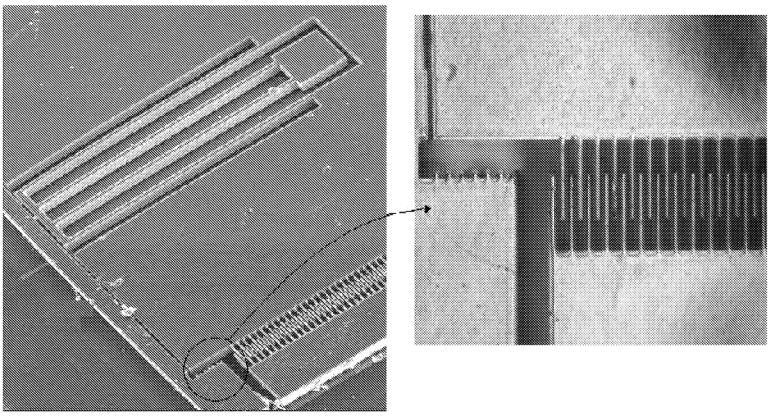

Fig.9 Prevention of stiction by reducing contact area in microaccelerometer[20]

(1) Eliminate release stiction by effectively reversing the shape of the water meniscus which forms underneath microstructures during the drying process. This effect can be quantified by measuring the water contact angle on these surfaces. The water contact angle increases from $< 30°$ on SiO_2 surfaces to $\geq 110°$ on SAM-coated surfaces.

(2) Reduce in-use stiction, quantified by apparent work of adhesion, by four orders of magnitude with respect to the conventional oxidized release process.

(3) Eliminate the need for large input signals (or mechanical probing) in the start-up phase in microengines.

(4) Reduce friction in microengines (static friction value of 0.08 vs. 2.3 for oxide-coated surfaces).

(5) Reduce wear significantly (over 40 million operation cycles have been achieved in touch-mode electrostatic actuators).

(6) Survive some packaging environments (thermally stable to 400°C in various, including oxygen containing, environments).

Several classes of organic films have been explored. These include alkyi- and perfluoroalkytrichlorosilane SAMs, dichlorosilane- and alkene-based molecular films. Among these classes of films, the most widely used is the octadecyltrichlorosilane-based SAM (OTS SAM). OTS SAM has been proved to be effective in alleviating release-related stiction and to be a potential post-release anti-stiction lubricant. Friction and wear studies of OTS SAM have also been carried out[26]. Though low friction coefficients of OTS SAM are recorded, poor load-carrying capacity and anti-wear ability are also shown. Lower values for the apparent work of adhesion were reported for 1H, 1H, 2H, 2H-perfluorodecyltrichlorosilane (FDTS) in comparison to OTS[27]. The dimethyldichlorosilane (DDMS) monolayer has also been proposed as a promising surface coating for MEMS. Table 3 gives a variety of properties for some anti-stiction coatings. The contact angle, being a thermodynamic quantity, reflects the surface and interfacial energies. Thus the contact angle of the surface plays an important role in stiction during evaporation after the final rinsing. The hydrophobic surfaces modified by the SAM coatings reduce the surface energy, and this increases the detachment length. Similar to Eq.(6), the critical detachment length of cantilever to be adhered to the substrate is

$$l_{\text{crit}} = \left(\frac{3}{8}\frac{Et^3h^2}{\gamma_{\text{la}}(\cos\theta_1 + \cos\theta_2)}\right)^{1/4} \tag{16}$$

Table 3 Comparison of physical properties among various surface treatments

Surface treatment	Contact angle		Work of adhesion /(mJ·m^{-2})	Coeff. of static friction	Thermal stability in air	Particulate formation	Selective to Si
	water	hexadecane					
OTS	110°	38°	0.012	0.07	225°C	high	no
FDTS	115°	68°	0.005	0.10	400°C	very high	no
DDMS	103°	38°	0.045	0.28	400°C	low	no
octadecene	104°	35°	0.009	0.05	200°C	negligible	yes
oxide	0∼30°	0∼20°	20	1.1	–	–	–

where γ_{la} is the surface tension of the liquid, θ_1 is the contact angle between the beam and the liquid, and θ_2 is the contact angle between the liquid and the substrate. Reducing γ_{la} and increasing θ_1 and θ_2 enhance the detachment length of the cantilever.

Preliminary experimental results in Ref.[28] indicate a significant reduction in the coefficient of static friction upon coating C_{60}-SAMs on 3-Aminopropyltrethoxysilane (APS) modified silicon (as shown in Fig.10). Lower surface energy is one of the reasons for the reduction of the coefficient of the friction and wear. Monolayer films of heptafluorobutyric anhydride (HFBA)[29] and n-Alkanoic acid[30] were prepared on polyethyleneimine (PEI) coated single crystal silicon (SCS) and glass substrates, respectively. The surface energies were lowered, therefore, these monolayers are useful for anti-stiction and lubrication in MEMS.

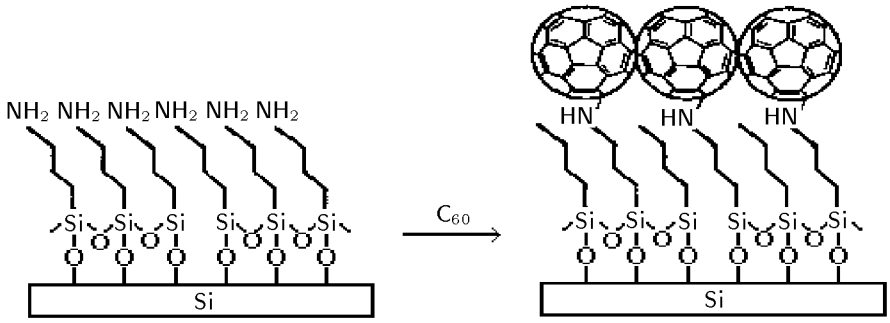

Fig.10 Formation of C_{60}-SAMs on APS modified Si substrate

A novel superhydrophobic ultra-thin film with contact angle of 166° was prepared[31] by stearic acid (STA) chemically adsorbed onto the polyethyleneimine (PEI) coated aluminum wafer. Composite interface between the water droplet and the rough needle-like surface was responsible for the super water-repellent property. It was found that a close relationship existed between the surface morphology and the contact angle. The ultra-thin film has a weak contact angle hysteresis with the advancing and receding contact angle about 168° and 156°, respectively. However, if the water droplet was placed onto the surface keeping static for a long times, the contact mode might be changed from composite interface into noncomposite interface, and then generate a large angle hysteresis. Figure 11 shows the superhydrophobic STA monolayer surface with contact angle of 166° (shown in Fig.12).

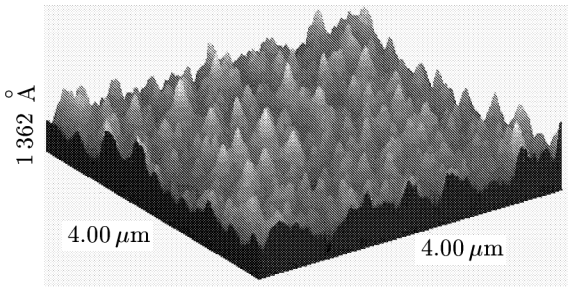

Fig.11 AFM 3D images of STA monolayers on PEI-coated polished aluminum surface with rough needle-like structure

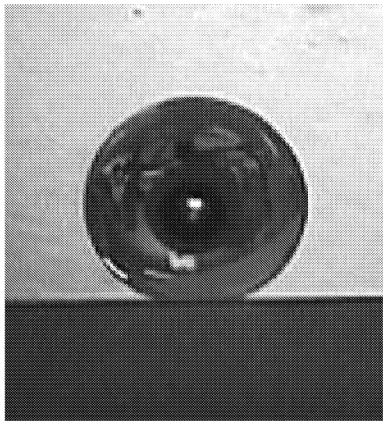

Fig.12 Shape of water droplet on the rough STA monolayer surface (volume of the droplet is 3 μL)

4 DISCUSSION AND CONCLUDING REMARKS

The extremely high surface-to-volume ratio of MEMS makes interfacial stiction, friction and wear significant factors in determining device reliability[32]. These important problems must be solved in a near future for production of reliable and long lasting MEMS[33]. Some criteria for sticiton of microstructures with substrate have been reviewed in this paper. Though some physical models have been established, great efforts including experiments, molecular dynamics (MD) simulation and theoretical analysis

are still needed to better understand the mechanisms of sticiton[34~37], jump-in-contact (JC) and jump-out-of-contact, and adhesion hysteresis.

From the various expressions of elasocapillary and peel numbers, we know that there are generally three ways for anti-stiction: (1) minimizing the work of adhesion by using SAMs and other low-surface-energy coatings; (2) making the surface hydrophobic or increasing the contact angle; and (3) roughening the surface and reducing the contact area (e.g., by making some dimples). Of all the above anti-stiction methods, the low-surface-energy coatings are the most effective and reliable[38]. The monolayer technique is especially attractive in the sense that it solves both capillary pull and stiction problems with only one application.

SAM is an effective measure to reduce the surface energy and prevent stiction in MEMS and NEMS. Various SAMs potentially used in MEMS have been reviewed and compared in the second part of this paper. Despite the large number of anti-stiction coatings now available[38], it is difficult to single out one treatment as the best surface coating.

The demand for reliable anti-stiction methods of MEMS and NEMS structures is essentially unlimited. A wear-resistant conformal anti-stiction coating remains highly desirable, and the ability to tailor the electrical properties of SAM for electrostatic actuators appears to be very important[39].

REFERENCES

1 Maboudian R, Ashurst WR, Carraro C. Tribological challenges in micromechanical systems. *Tribol Lett*, 2002, 12(2): 95~100

2 Ashurst WR, Yau C, Carraro C, et al. Alkene based monolayer films as anti-stiction coatings for polysilicon MEMS. *Sensors Actuators*, 2001, A91(3): 239~248

3 Ashurst WR, Yau C, Carraro C, et al. Dichlorodimethylsilane as an anti-stiction monolayer for MEMS: A comparison to the octadecyltrichlosilane self-assembled monolayer. *J Microelectromech Syst*, 2001, 10(1): 41~49

4 Li QY, Yu SW. A model of computation of elastic and plastic contact considering adhesion effect. *Int J Nonlinear Sci Numerical Simulation*, 2002, 3(3-4): 599~602

5 Zhao YP. Morphological stability of epitaxial thin elastic films by van der Waals force. *Arch Appl Mech*, 2002, 72(1): 77~84

6 Zhao YP, Li WJ. Surface stability of epitaxial elastic films by the Casimir force. *Chin Phys Lett*, 2002, 19(8): 1161~1163

7 Kim BH, Chung TD, Oh CH, et al. A new organic modifier for anti-stiction. *J Microelectromech Syst*, 2001, 10(1): 33~40

8 Zhang LX, Zhang JW, Zhao YP, et al. Failure modes of doubly supported capacitive RF MEMS switches. *Int J Nonlinear Sci Numerical Simulation*, 2002, 3(3-4): 353~356

9 Mastrangelo CH, Hsu CH. Mechanical stability and adhesion of microstructures under capillary forces-part I and part II. *J Microelectromech Syst*, 1993, 2(1): 33~55

10 De Boer MP, Michalske TA. Accurate method for determining adhesion of cantilever beams. *J Appl Phys*, 1999, 86(2): 817~827

11 Wang LS, Zhao YP. Effect of surface roughness on the adhesion of microstructures. *Tribology*, 2002, 22(4s): 339~343 (in Chinese)

12 Fuller KNG, Tabor D. The effect of surface roughness on the adhesion of elastic solids. *Proc R Soc Lond*, 1975, A345(1641): 327~342

13 Buks E, Roukes ML. Stiction, adhesion energy, and the Casimir effect in micromechanical systems. *Phys Review*, 2001, B63(3): 033402

14 Israelachvili JN. Intermolecular and Surface Forces. 2nd ed. London: Academic Press, 1991

15 Boström M, Sernelius BE. Fractional van der Waals interaction between thin metallic films. *Phys Rev*, 2000, B61(3): 2204~2210

16 Bordag M, Mohideen U, Mostepanenko VM. New developments in the Casimir effect. *Phys Rep*, 2001, 353(1-3): 1~205

17 Serry FM, Walliser D, Maclay GJ. The role of the casimir effect in the static deflection and stiction of membrane strips in micromechanical systems (MEMS). *J Appl Phys*, 1998, 84(5): 2501~2506

18 Johnstone RW, Parameswaran M. Theoretical limits on the freestanding length cantilevers produced by surface micromachining technology. *J Micromech Microeng*, 2002, 12(6): 855~861

19 Van Spengen WM, Puers R, de Wolf I. A physical model to predict stiction in MEMS. *J Micromech Microeng*, 2002, 12(5): 702~713

20 Wang LS. Microaccelerometers: design, simulation and mechanical analysis. [MS Thesis], Institute of Mechanics, Chinese Academy of Sciences, 2001 (in Chinese)

21 Fan LS. Integrated Micromachinery-Moving Structures in Silicon Chips. [PhD Thesis], University of California, Berkeley, 1990

22 Maboudian R. Surface processes in MEMS technology. *Surf Sci Rep*, 1998, 30(6-8): 207~269

23 Bhushan B, Dandavate C. Thin-film friction and stiction studies using atomic force microscopy. *J Appl Phys*, 2000, 87(3): 1201~1210

24 Åström R, Mutikainen R, Kuisma H, et al. Effect of alkylsilane coating on sliding wear of silica-silicon

contacts with small amplitude motion. *Wear*, 2002, 253(7-8): 739∼745

25 Kim JM, Baek CW, Park JH, et al. Continuous anti-stiction coatings using self-assembled monolayers for gold microstructures. *J Micromech Microeng*, 2002, 12(5): 688∼695

26 Ren SL, Yang SR, Zhao YP, et al. Friction and wear studies of octadecyltrichlorosilane SAM on silicon. *Tribol Lett*, 2002, 13(4): 233∼239

27 Srinivasan U, Houston MR, Howe RT, et al. Alkylsiloxane-based self-assembled monolayers for stiction reduction in silicon micromachines. *J Microelectromech Syst*, 1998, 7(2): 252∼260

28 Ren SL, Zhao YP, Yang SR, et al, Preparation and tribological properties of C_{60}-terminated self-assembled monolayers. *J Mech Strength*, 2001, 23(4): 507∼510 (in Chinese)

29 Ren SL, Yang SR, Wang JQ, et al. Preparation and structure of HFBA monolayer on PEI-coated single crystal silicon substrate. *Acta Chimica Sinica*, 2001, 59(11): 1894∼1897 (in Chinese)

30 Ren SL, Yang SR, Wang B, et al. Preparation and tribology studies of alkyl carboxylic acid monolayer films on PEI-coated glass substrate. *Chin J Mater Res*, 2002, 16(1): 46∼50 (in Chinese)

31 Ren SL, Yang SR, Zhao YP, et al. Morphology correlation to the superhydrophobicity in an organic thin film on rough Al. *Int J Nonlinear Sci Numerical Simulation*, 2002, 3(3-4): 785∼788

32 De Boer MP, Knapp JA, Michalske TA, et al. Adhesion hysteresis of silane coated microcantilevers. *Acta Mater*, 2000, 48(18-19): 4531∼4541

33 Rymuza Z. Control tribological and mechanical properties of MEMS surface. Part 1: critical review. *Microsyst Technol*, 1999, 5(4): 173∼180

34 Wen SZ. Nanotribology. Beijing: Tsinghua University Press, 1998

35 Zhao YP, Yu TX. Failure modes of MEMS and microscale adhesive contact theory. *Int J Nonlinear Sci Numerical Simulation*, 2000, 1(5): 361∼371

36 Zhao YP, Wang LS, Sun KH. Tabor number, adhesion parameter and elastic theory of micro-scale adhesive contact. *Advances in Mechanics*, 2000, 30(4): 529∼537 (in Chinese)

37 Zhao YP. Microscale plastic adhesive contact theory. In: Advances in Plasticity and Geodynamics, Xu BY, Huang ZP eds. Beijing: World Publishing Corporation, 2000. 118∼124 (in Chinese)

38 Mastrangelo CH. Adhesion-related failure mechanisms in micromechanical devices. *Tribol Lett*, 1997, 3(3): 223∼238

39 Maboudian R, Ashurst WR, Carraro C. Self-assembled monolayers as anti-stiction coatings for MEMS: characteristics and recent development. *Sensors Actuators*, 2000, A82(1-3): 219∼223